optica

Phase sensing beyond the standard quantum limit with a variation on the SU(1,1) interferometer: supplementary material

BRIAN E. ANDERSON[1], PRASOON GUPTA[1], BONNIE L. SCHMITTBERGER[1], TRAVIS HORROM[1], CARLA HERMANN-AVIGLIANO[1], KEVIN M. JONES[2], AND PAUL D. LETT[1,3,*]

[1]Joint Quantum Institute, National Institute of Standards and Technology and the University of Maryland, College Park, MD 20742
[2]Department of Physics, Williams College, Williamstown, Massachusetts 01267
[3]Quantum Measurement Division, National Institute of Standards and Technology, Gaithersburg, MD 20899
[*]Corresponding author: paul.lett@nist.gov

Published 24 May 2017

This document provides supplementary information to "Phase sensing beyond the standard quantum limit with a variation on the SU(1,1) interferometer," https://doi.org/10.1364/optica.4.000752. The sensitivity of an SU(1,1)-type phase measurement device depends on both the phase-sensing quantum state and the choice of detection scheme. Here, we provide a theoretical framework for analyzing the phase sensitivity of the full and truncated SU(1,1) interferometers using both intensity and homodyne detection schemes, as summarized in the main article. We show that homodyne detection is optimal for a seeded SU(1,1)-type phase measurement device. We also discuss the effect of losses on the measured phase sensitivity as well as our experimental techniques for verifying the standard quantum limit. © 2017 Optical Society of America

https://doi.org/10.1364/optica.4.000752.s001

1. DERIVING THE PHASE SENSITIVITY

We consider two input modes a and b, as shown in Fig. S1. Mode a is seeded with a coherent state, where $\langle \hat{a}_0^\dagger \hat{a}_0 \rangle = |\alpha|^2$ is the seed photon number, and mode b is seeded with a vacuum state [1]. The input modes, described by $\vec{v}$, undergo a squeezing operation $\hat{U}$, as shown in Fig. S1, where for a squeezing parameter r,

$$\hat{U}\vec{v} = \begin{pmatrix} \cosh(r) & 0 & 0 & \sinh(r) \\ 0 & \cosh(r) & \sinh(r) & 0 \\ 0 & \sinh(r) & \cosh(r) & 0 \\ \sinh(r) & 0 & 0 & \cosh(r) \end{pmatrix} \begin{pmatrix} \hat{a}_0 \\ \hat{a}_0^\dagger \\ \hat{b}_0 \\ \hat{b}_0^\dagger \end{pmatrix}. \quad \text{(S1)}$$

The probe (seeded) arm undergoes a phase shift $e^{i\phi}$. We treat loss in terms of beam splitters of transmission η_j, as shown in Fig. S1, where each beam splitter also injects vacuum noise, described by the mode operators $\hat{c}_0$, $\hat{d}_0$, $\hat{e}_0$, and $\hat{f}_0$. For the full SU(1,1) interferometer, the beams undergo a second squeezing operation of squeezing parameter s (typically $s = r$). For the truncated SU(1,1) interferometer, $s = 0$. At the output of the second squeezer, the modes of the upper (probe) and lower (conjugate) arms are described by the operators $\hat{a}_f$ and $\hat{b}_f$, where

$$\hat{a}_f = i\hat{e}_0\sqrt{1-\eta_{p2}} + \sqrt{\eta_{p2}}\Big\{\cosh(s)\Big[i\hat{c}_0\sqrt{1-\eta_{p1}} + \sqrt{\eta_{p1}}\left(\hat{a}_0 e^{i\phi}\cosh(r) + e^{i\phi}\sinh(r)\hat{b}_0^\dagger\right)\Big] + -\sinh(s)\left[\sqrt{\eta_{c1}}\left(\hat{a}_0\sinh(r) + \cosh(r)\hat{b}_0^\dagger\right) - i\sqrt{1-\eta_{c1}}\hat{d}_0^\dagger\right]\Big\}, \quad \text{(S2)}$$

and

$$\hat{b}_f = i\hat{f}_0\sqrt{1-\eta_{c2}} + \sqrt{\eta_{c2}}\Big\{\cosh(s)\Big[i\hat{d}_0\sqrt{1-\eta_{c1}} + \sqrt{\eta_{c1}}\left(\hat{b}_0\cosh(r) + \sinh(r)\hat{a}_0^\dagger\right)\Big] + -\sinh(s)\Big[\sqrt{\eta_{p1}}\left(\hat{b}_0 e^{-i\phi}\sinh(r) + e^{-i\phi}\cosh(r)\hat{a}_0^\dagger\right) + -i\sqrt{1-\eta_{p1}}\hat{c}_0^\dagger\Big]\Big\}. \quad \text{(S3)}$$

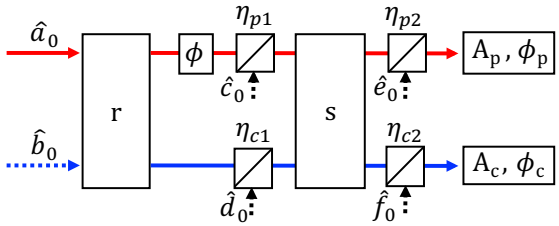

Fig. S1. A schematic of the model used to derive the phase sensitivity. A coherent state and a vacuum state undergo a squeezing operation of squeezing parameter r. The probe (upper) arm undergoes a phase shift ϕ. Loss is modeled using beamsplitters of reflectivity $1-\eta_j$. In the full SU(1,1) interferometer, the beams undergo a second squeezing operation of squeezing parameter s. Homodyne detection is characterized by a classical amplification A_j and a phase ϕ_j.

We then give the detector for the probe (conjugate) arm a classical amplification A_p (A_c) and a homodyne phase ϕ_p (ϕ_c). For the truncated SU(1,1) interferometer, we take $A_p = A_c = 1$.

A. Quadrature detection

For homodyne detection, we define the quadrature operators $\hat{j}_p = A_p\left(e^{-i\phi_p}\hat{a}_f + e^{i\phi_p}\hat{a}_f^\dagger\right)$ and $\hat{j}_c = A_c\left(e^{-i\phi_c}\hat{b}_f + e^{i\phi_c}\hat{b}_f^\dagger\right)$ for the probe and conjugate arms, respectively. The joint quadrature operator is $\hat{J} = \hat{j}_p + \hat{j}_c$. The sensitivity $\Delta\phi$ is then calculated with the inputs and the operator transformations in Eqs. S2 and S3 from the variance (see Eq. (1) in the main paper)

$$\left(\Delta^2\phi\right)_J = \frac{\langle J^2\rangle - \langle J\rangle^2}{\left|\partial_\phi \langle J\rangle\right|^2}. \tag{S4}$$

To compare the truncated SU(1,1) interferometer ($s=0$) and the full SU(1,1) interferometer ($s=r$), we consider $A_p = A_c = 1$, $\eta_{p1} = \eta_{c1} = \eta$, and $\eta_{p2} = \eta_{c2} = 1$. For the truncated SU(1,1) interferometer, Eq. S4 becomes

$$\Delta^2\phi_{\text{tSUI}} = \frac{\text{sech}^2(r)\left[1-\eta+\eta\cosh(2r)+\eta\cos(\phi_p-\phi+\phi_c)\sinh(2r)\right]}{2|\alpha|^2\eta\sin^2(\phi_p-\phi)}. \tag{S5}$$

In the case where $\phi = 0$ and $\phi_c = \pi/2$, Eq. S5 reduces to Eq. 3 in the main paper. In the case $\eta = 1$, Eq. (S4) gives rise to curves (i) and (v) in Fig. 2 of the main paper, where $r = \cosh^{-1}(\sqrt{G})$ for gain G. In general, one can show that the minimum $\Delta^2\phi_{\text{tSUI}}$ occurs for $\phi_c = \pi/2$ and $\phi_p - \phi = \pi/2$, so that the optimal sensitivity for the truncated SU(1,1) interferometer in this case is

$$\Delta^2\phi_{\text{tSUI}} = \frac{\text{sech}^2(r)\left[1-\eta+\eta\cosh(2r)-\eta\sinh(2r)\right]}{2|\alpha|^2\eta}. \tag{S6}$$

For the full SU(1,1) interferometer, Eq. S4 becomes

$$\Delta^2\phi_{\text{SUI}} = \Big(2-4\eta-\text{sech}^2(r)+2\eta\Big[\cosh(2r)+\text{sech}^2(r)+ -2\cos(\phi)\sinh^2(r)\Big]+\eta\cos(\phi_p+\phi_c)\cos(\phi)\text{sech}(r)\sinh(3r)+ \tanh(r)\Big\{2\eta\sin(\phi_p+\phi_c)\sin(\phi)+ -\cos(\phi_p+\phi_c)\left[2-2\eta+\eta\cos(\phi)+2\eta\cosh(2r)\right]\Big\}\Big)\Big/ \Big\{2|\alpha|^2\eta\left[\cosh(r)\sin(\phi_p-\phi)+\sin(\phi_c+\phi)\sinh(r)\right]^2\Big\}. \tag{S7}$$

One can numerically optimize over all ϕ, ϕ_p, and ϕ_c to show that the optimal (minimum) $\Delta^2\phi_{\text{SUI}}$ is equivalent to that of the truncated SU(1,1) interferometer for all r. For any ϕ, the local oscillator phases ϕ_p and ϕ_c can be adjusted to achieve this optimal phase sensitivity. In the special case where $\phi = 0$, there is a straightforward analytic solution, where Eq. S7 simplifies to

$$\Delta^2\phi_{\text{SUI}} = \frac{\text{sech}^2(r)(2\eta-1)+2(\eta-1)\left[\cos(\phi_p+\phi_c)\tanh(r)-1\right]}{2|\alpha|^2\eta\left[\cosh(r)\sin(\phi_p)+\sinh(r)\sin(\phi_c)\right]^2}. \tag{S8}$$

In this case, the sensitivity is again optimized by detecting the phase quadrature of each field, where $\phi_p = \phi_c = \pi/2$. The optimal sensitivity for the full SU(1,1) interferometer in this case is then $\Delta^2\phi_{\text{SUI}} = \Delta^2\phi_{\text{tSUI}}$ from Eq. S6.

In addition, one can show that Eqs. S6 and S8 are bounded from below by $1/\mathcal{F}_Q$, where $\mathcal{F}_Q$ is defined in Eq. 4 of the main paper. In the limit where $r \to \infty$, $\Delta^2\phi_{\text{SUI}} = \Delta^2\phi_{\text{tSUI}}$ asymptotically approaches $1/\mathcal{F}_Q$, which defines the best achievable sensitivity.

B. Direct detection

For direct intensity detection, we define the number operators $\hat{n}_p = A_p\hat{a}_f^\dagger\hat{a}_f$ and $\hat{n}_c = A_c\hat{b}_f^\dagger\hat{b}_f$ for the probe and conjugate arms, respectively, where we simply take A_p and A_c to be 1 or 0 depending on which detector(s) are on/off. We are interested in the sum $\hat{N} = \hat{n}_p + \hat{n}_c$. The phase sensitivity using direct detection is then calculated from the square root of the variance

$$\left(\Delta^2\phi\right)_N = \frac{\langle N^2\rangle - \langle N\rangle^2}{\left|\partial_\phi\langle N\rangle\right|^2}. \tag{S9}$$

To derive the case of a single detector in the conjugate arm, we take $A_p = 0$. In the case of no loss ($\eta_{p1} = \eta_{c1} = \eta_{p2} = \eta_{c2} = 1$), the variance of the phase estimation using number detection in the most sensitive ($\phi = 0$) case for just the conjugate detector with $s = r$ and $A_c = 1$ is

$$\left(\Delta^2\phi\right)_{N,\text{conj}} = \frac{\text{csch}^2(2r)}{|\alpha|^2}, \tag{S10}$$

which gives rise to curve (iii) in Fig. 2 of the main paper. Equation (S10) is also equivalent to $\left(\Delta^2\phi\right)_J$ with $A_p = 0$ (only the conjugate homodyne detector) at the point of optimal sensitivity, corresponding to curve (ii) in Fig. 2 of the main paper.

For detecting both modes from the interferometer, we take $A_p = A_c = 1$. In the case of no loss and $s = r$, the variance of the phase estimation using number detection at the best operating point is

$$\left(\Delta^2\phi\right)_{N,\text{probe+conj}} = \frac{\text{csch}^4(2r)\left[2\cosh(4r)+\sqrt{\cosh(8r)}-1\right]}{2|\alpha|^2}, \tag{S11}$$

which gives rise to curve (iv) in Fig. 2 of the main paper.

C. Operating with the best sensitivity

To analyze the signal-to-noise ratio improvement (SNRI) as a function of operating point, it is useful to determine the SNRI as a function of the relative homodyne phases ϕ_p and ϕ_c. One can show from Eq. S4 that

$$\Delta^2\phi_{\text{tSUI}} = \frac{2\eta+(1-2\eta)\,\text{sech}^2(r)+2\eta\cos(\phi_p+\phi_c)\tanh(r)}{2|\alpha|^2\eta\sin^2(\phi_p)}. \tag{S12}$$

In the special case where $\phi_c = \pi/2$, this reduces to Eq. 3 in the main paper. From Eq. S12 and the definitions of $\Delta^2\phi_{\rm coh}$ and SNRI in the main paper, one obtains Fig. S2(a), which shows the SNRI as a function of ϕ_p and ϕ_c for $\eta = 1$. Figure S2(b) shows the corresponding $\langle j_p \rangle$ and $\langle j_c \rangle$. Thus, the best SNRI occurs when ϕ_p and ϕ_c are locked to their phase quadratures (*i.e.*, the zero-crossings of $\langle j_p \rangle$ and $\langle j_c \rangle$), and when $\langle j_p \rangle$ and $\langle j_c \rangle$ have the same slope. We investigate the SNRI as a function of operating point in the main paper by locking ϕ_c to its phase quadrature and scanning ϕ_p.

2. DISCUSSION OF LOSSES

As was shown in Refs. [2, 3], the sensitivity of the full SU(1,1) interferometer is inhibited by two types of losses: internal (η_{p1}, η_{c1}) and external (η_{p2}, η_{c2}). Examples of external losses include detector inefficiencies or imperfect visibility in homodyne detection, and internal losses include all losses inside and between the 4WM processes, such as absorption, optical loss, and imperfect mode-matching in the second 4WM process. One can show that internal and external losses have different effects on the sensitivity, and that internal losses are more detrimental [2]. With $\eta_{p1} = \eta_{c1} = \eta_{\rm int}$ and $\eta_{p2} = \eta_{c2} = \eta_{\rm ext}$, the variance of the phase estimation $\left(\Delta^2\phi\right)_J$ depends differently on $\eta_{\rm int}$ vs. $\eta_{\rm ext}$. Specifically, for no external losses,

$$\left(\Delta^2\phi\right)_{J,\,\eta_{\rm ext}=1} = \frac{e^{-r}\,\mathrm{sech}\,(r)\left[1+\tanh(r)-2\eta_{\rm int}\tanh(r)\right]}{2\eta_{\rm int}|\alpha|^2}. \tag{S13}$$

For no internal losses,

$$\left(\Delta^2\phi\right)_{J,\,\eta_{\rm int}=1} = \frac{2}{\eta_{\rm ext}|\alpha|^2\left[1+\cosh(2r)+\sinh(2r)\right]^2}. \tag{S14}$$

For a gain of 3.3 ($r \approx 1.2$), $|\alpha|^2\left(\Delta^2\phi\right)_{J,\,\eta_{\rm ext}=1}$=0.05 for $\eta_{\rm int} = 0.8$, and $|\alpha|^2\left(\Delta^2\phi\right)_{J,\,\eta_{\rm int}=1}$=0.02 for $\eta_{\rm ext} = 0.8$. Thus, the sensitivity is more robust against external losses than internal losses. The truncated SU(1,1) interferometer offers an advantage over the full version in that it eliminates any internal loss associated with the second 4WM process. A disadvantage of the truncated SU(1,1) interferometer compared to the full version is that all losses are internal, so that one must use high quantum efficiency detectors and achieve high homodyne visibilities to minimize loss.

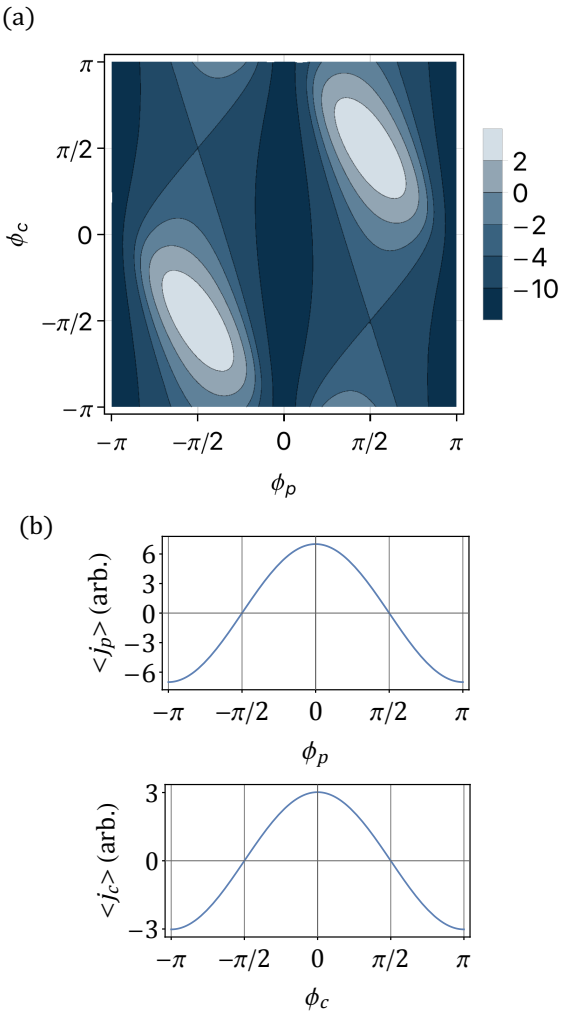

Fig. S2. (a) The SNRI as a function of HD phases ϕ_p and ϕ_c in the case where $|\alpha|^2 \gg 1$ and $r = 0.46$, which corresponds to 4 dB of squeezing. The legend defines the SNRI on a dB scale. The regions of best phase sensitivity are shown in light colors. (b) The probe and conjugate HD signals ($\langle j_p \rangle$ and $\langle j_c \rangle$) as functions of the relative phases ϕ_p and ϕ_c considered in (a). This shows that the best SNRI is achieved by locking ϕ_p and ϕ_c to the zero crossing point with the same slope.

3. VERIFYING THE SQL

We perform auxiliary experiments to compare the SNR measured with coherent beams to that expected for the truncated Mach-Zehnder interferometer. For our two-homodyne setup, we expect $\mathrm{SNR}_{\rm coh} = (\delta\phi)^2 N_p$, where $\delta\phi$ is the RMS amplitude of the EOM phase modulation and $N_p = 2\eta_{\rm coh}\rho P/eB$, where $\eta_{\rm coh}$ is a loss parameter, $\rho = 0.64$ A/W is the responsivity for an ideal (100 % quantum efficiency) detector at 795 nm, $P = 400 \pm 20$ nW is the power in the probe beam, e is the electric charge, and B is the "equivalent noise bandwidth." The loss parameter $\eta_{\rm coh}$ includes the detector quantum efficiency 0.9, the homodyne visibility (≈ 0.95 for these experiments), and separation from electronic noise (20 dB separation, hence negligible), from which we expect $\eta_{\rm coh} \approx 0.8$. This $\eta_{\rm coh}$ (≈ 20 % loss) differs from the loss parameter $\eta = 0.65$ in the main paper (≈ 35 % loss) because it only accounts for detector loss, whereas η also includes losses in the quantum state preparation. The apparent SNR shown on the spectrum analyzer trace (Fig. 4a in the main paper) needs a correction to account for the different ways in which broadband and narrowband signals are processed (see for example Ref. [4]) and the resolution bandwidth converted to bandwidth to account for the filter function employed. We use the built-in software corrections on the spectrum analyzer to determine the corrected SNR in a bandwidth of 30 kHz.

In the case where $\delta\phi = 1.7 \pm 0.2$ mrad, we find that our corrected $\mathrm{SNR}_{\rm coh} \approx 22.5$ dB. Given the uncertainties in $\delta\phi$, P, and the spectrum analyzer calibration, this agrees with the expected $\eta_{\rm coh} \approx 0.8$. Thus we conclude that the measured SQL agrees with the expected limit for a truncated Mach-Zehnder interferometer.

In the data shown in Fig. 4 of the main paper, the homodyne visibility was ≈ 98 %, and the electronic noise floor separation was ≈ 18 dB, which corresponds to detector losses of $\approx$ 15%. If the coherent state measurements could have been made with

a perfect detector, then the SNR_{coh} would have increased by ≈ 1 dB, and the corresponding SNRI over the idealized SNR_{coh} would still have been 3 dB.

REFERENCES

1. B. E. Anderson, B. L. Schmittberger, P. Gupta, K. M. Jones, and P. D. Lett, "Optimal phase measurements with bright and vacuum-seeded SU(1,1) interferometers," to be published.
2. A. M. Marino, N. V. Corzo Trejo, and P. D. Lett, "Effect of losses on the performance of an SU(1,1) interferometer," Phys. Rev. A **86**, 023844 (2012).
3. F. Hudelist, J. Kong, C. Liu, J. Jing, Z. Y. Ou, and W. Zhang, "Quantum metrology with parametric amplifier-based photon correlation interferometers," Nat. Commun. **5**, 3049 (2014).
4. Agilent Technologies, Inc. "Agilent Spectrum and Signal Analyzer Measurements and Noise, Application Note." 5966-4008E (2012).